Spatiotemporal nematodynamics in wormlike micelles en route to rheochaos

Rajesh Ganapathy, Sayantan Majumdar, and A. K. Sood
Department of Physics, Indian Institute of Science, Bangalore 560012, India
(Received 14 June 2007; revised manuscript received 25 July 2008; published 21 August 2008)

We show through polarized light scattering experiments the spatially inhomogeneous orientational dynamics for shear-thinning wormlike micellar gels (cetyltrimethylammonium tosylate+sodium chloride+H_2O) en route to rheochaos. For shear rates in the plateau of the flow curve, we see alternating bright and dark birefringent stripes stacked along the vorticity. The orientational order in adjacent bands is predominantly oriented at +45° and −45° to the flow ($\mathbf{v}$) in the ($\mathbf{v},\nabla\mathbf{v}$) plane, respectively. We have made an attempt to correlate the observed orientational ordering in terms of the two-dimensional Taylor-like velocity rolls in a gradient banding fluid. The bands show spatial motion along the vorticity, and the orientation dynamics of the interface delineating adjacent bands completely correlates with the temporal dynamics of the stress. Furthermore, the observed spatial dynamics of the interfaces of the rolls depends crucially on the gap width of the Couette cell.

DOI: 10.1103/PhysRevE.78.021504 PACS number(s): 83.80.Qr, 82.70.Uv, 83.60.Wc, 83.85.Ei

I. INTRODUCTION

Rheochaos—irregular time dependence in the stress at constant shear rate or vice versa—is a flow instability that occurs at practically zero Reynolds number in systems whose flow curve is intrinsically nonmonotonic or multivalued [1]. For shear-thinning wormlike micellar gels, such flow curves emerged naturally from a model due to Spenley *et al.* [2] and were later confirmed by flow birefringence and NMR experiments [3]. In the model of [2], the stress decreases when shear rate is increased past a threshold value. Homogeneous flow is then unstable and the system splits into bands with a stable interface normal to the flow gradient direction: a high shear rate band (oriented phase) and a low shear rate band (isotropic phase) coexist at a common stress. NMR velocimetry and rheo-optical measurements, however, have shown that the band interface shows complex spatiotemporal dynamics, accompanied by stress or shear rate fluctuations [4]. In the case of shear-thickening wormlike micellar gels, bands of different stress, with interface normal to the vorticity direction, coexist at a common shear rate and again exhibit complex spatiotemporal dynamics [5]. In current theoretical models for rheochaos, spatial heterogeneity is thus a key ingredient [6–9]. These models predict rich spatiotemporal dynamics of the nematic-orientational-order–shear-band interface across the gap, and this is reflected in the temporal behavior of the stress. Typical of a nonlinear dynamical system with coupled spatial and temporal degrees of freedom, the complexity of the observed dynamics was predicted to depend on the system size [8].

In a recent experiment, the gradient-band interface was found to be unstable with respect to undulations with wave vector along the vorticity in a shear-thinning wormlike micellar gel (cetyltrimethylammonium bromide+$NaNO_3$ in water) [10]. This is intriguing because vorticity structuring has been associated with shear-thickening systems. The experiments did not show any temporal dynamics in the measured stress. It is also worth mentioning here that *transient* vorticity bands arising from two-dimensional (2D) Taylor-like velocity rolls were recently seen in shear-thinning rodlike virus suspensions due to inhomogeneities caused from an underlying paranematic-nematic phase separation [11]. The motivation for the present experiments is to understand the nature of the spatiotemporal dynamics as a system approaches a chaotic state. Specifically, we wish to address the following: (1) The dynamics of vorticity structures, if present in a system that shows the route to rheochaos, and (2) the influence of system size on the spatial dynamics of the nematic order. To this end, we have carried out polarized scattering experiments to quantify the orientational dynamics for a shear-thinning wormlike micellar gel of cetyltrimethylammonium tosylate (CTAT) in the presence of salt sodium chloride (NaCl). This system shows one of the classic routes to chaos, namely, type-II intermittency, and the nematic order is found to be strongly correlated with the stress dynamics [12–14]. Unlike the earlier small-angle light-scattering (SALS) measurements [12], which probed only the temporal behavior of the nematic order, the present experiments probe the nematic order as a function of space and time over the entire gap of the Couette cell en route to chaos. Also, our scattering geometry (imaging done in the $\nabla\mathbf{v}$, $\nabla\times\mathbf{v}$ plane) differs from that of Kang *et al.* (imaging done in the $\mathbf{v}$, $\nabla\times\mathbf{v}$ plane) [11] and gives access to the cross section of vorticity structures across the gap. Our main results are shown in Figs. 1, 2, and 4, where we see alternating bright and dark birefringent structures along the vorticity direction. The vorticity structures show spatial motion along $\nabla\times\mathbf{v}$, and depending on the Couette gap width this may be accompanied by interface dynamics, delineating adjacent vorticity bands, along $\nabla\mathbf{v}$. The temporal behavior of the stress is determined by the spatial dynamics of the vorticity bands. These experimental observations can be understood in terms of 2D Taylor-like velocity rolls that have been predicted recently for a shear-thinning fluid.

II. EXPERIMENT

We will now describe our experiments and elaborate on the results. The preparation of CTAT 2 wt. % with 100 m*M* NaCl is discussed in detail in [12]. The experiments were carried out on a MCR 300 stress-controlled rheometer (Anton PAAR, Germany). For imaging experiments, we have used two homemade transparent Couette cells of gap 1 mm

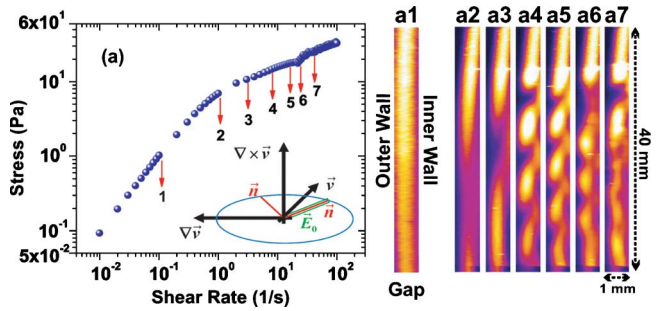

FIG. 1. (Color online) (a) Flow curve for CTAT 2 wt. % +100 mM NaCl in the 1 mm gap Couette cell. a1–a7: Scattered birefringence intensity profile at positions marked 1–7 on the flow curve. The positions of the outer wall, inner wall, and gap are marked for a1. The convention is the same for all images shown in the paper. Inset: shows a cartoon of the nematic in the $(\mathbf{v},\nabla\mathbf{v})$ plane (red lines) coupled to the incident laser polarization shown by green.

(inner cylinder diameter 18 mm, height 40 mm) and 2 mm (inner cylinder diameter 32 mm, height 16.5 mm). The outer cylinder is made of glass and is partially enclosed by a temperature-controlled water circulation chamber (approximately 1/4th of the glass cell is left exposed for performing scattering measurements). A thin sheet of laser light enters the shear cell along the $\nabla\times\mathbf{v}$ direction and illuminates the gap completely. A polarizer arrangement in front of the laser beam gives us the freedom of choosing any polarization in the $(\mathbf{v},\nabla\mathbf{v})$ plane. This way the incident polarization can be made to couple strongly with structures of a given orientation in this plane. The imaging was done at 90° in the $(\nabla\mathbf{v},\nabla\times\mathbf{v})$ plane using a CCD camera (UNIQ 1830CL, 1024×1024 pixels, maximum frame rate ~30 frames per second). For stress relaxation measurements, a zoom lens captured ≈30% of the height in the 1 mm gap Couette cell, and the complete height for the 2 mm gap cell. A wide-angle lens was used to capture the complete height in the 1 mm gap Couette cell during measurements of the flow curve. The optics was mounted on XYZ stages to facilitate scanning of different regions of the Couette cell. All measurements were carried out at a controlled temperature of 26.5 °C. Flow curves and stress relaxation measurements using the homemade cell reproduced our earlier results [12]. The flow curves were measured in an upward strain rate sweep with a residence time of 120 s per data point under controlled shear rate as follows: starting from the lowest value of the shear rate, at each shear rate the stress is measured by averaging over 120 s. The stress relaxation measurements were done starting from rest for each measurement at a fixed shear rate. After measuring the stress time series at a fixed shear rate, the shear rate was reduced to zero, followed by a waiting time for 240 s before starting the next measurement of stress time series at the next higher value of the shear rate.

III. RESULTS

Figure 1(a) shows the flow curve for the CTAT 2 wt. % +100 mM NaCl in controlled-shear rate conditions for the

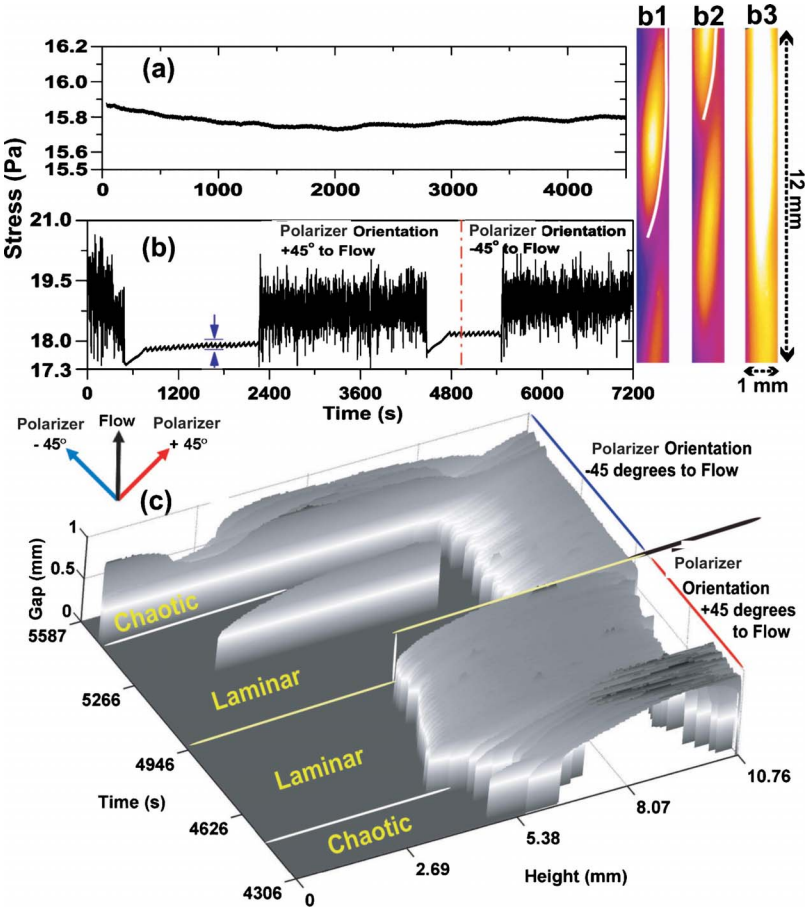

FIG. 2. (Color online) (a) Stress time series at $\dot{\gamma}=13\ \mathrm{s}^{-1}$ for the 1 mm gap Couette cell. (b) Stress time series at $\dot{\gamma}=18.5\ \mathrm{s}^{-1}$. The arrow indicates the amplitude ($a_0\approx0.8\%$). The dashed line indicates the time at which the incident laser polarization was changed from +45° (image: b1) to −45° (image: b2). b3 is the sum of b1 and b2. The thick white lines in b1 and b2 are the interface positions represented as a STP in (c).

1 mm gap Couette cell. For shear rates ($\dot{\gamma}$)>1 s^{-1}, there is a power-law deviation from a flat plateau ($\sigma \sim \dot{\gamma}^{\alpha}$, $\alpha=0.3$). This is a consequence of strong flow-concentration coupling [15]. Figure 1 (a1–a7) shows the evolution of the polarization response [16] in the gap as a function of shear rate for an incident light polarization at +45° to the flow. For shear rates in the Newtonian region, the scattered intensity is uniform in the gap [Fig. 1 (a1)] and rotation of the incident polarization causes no change in the scattered intensity. At the plateau onset, we see the emergence of alternating bright and dark inclined stripes stacked along $\nabla \times \mathbf{v}$ [Fig. 1 (a2)]. These bright regions correspond to local orientation parallel to the incident laser polarization. For an incident polarization at −45° to the flow, the structure observed is *complementary* to that observed at an incident polarization of +45°. For a polarizer orientation parallel to the flow, we observe that the scattered intensity in the gap is uniform since both nematic orientations (+45° and −45°) contribute equally. As the shear rate is increased, the wavelength of the vorticity bands decreases along $\nabla \times \mathbf{v}$ [Fig. 1 (a3–a5)] (see movie [17]). The vorticity structures are spatiotemporally stable up to $\dot{\gamma} \approx 19$ s^{-1}. For higher shear rates, the vorticity structures are destabilized (corresponds to the kink in the flow curve marked 6) and this is accompanied by spatial motion along the vorticity.

Figure 2(a) shows the stress time series at $\dot{\gamma}=13$ s^{-1} for the 1 mm gap Couette cell. This shear rate corresponds to point marked 4 on the flow curve and the vorticity structure is shown in Fig. 1 (a4). We observe no time dependence of the stress (amplitude $a_0<0.5\%$) and this is surprising in light of the fact that earlier measurements on the same system in a 2 mm gap Couette cell showed quasiperiodic oscillations ($a_0 \approx 8\%$) [12]. The vorticity structures were spatiotemporally stable during the run. At $\dot{\gamma}=18.5\ s^{-1}$ [Fig. 2(b)], the stress time series shows long intermittent chaotic bursts appearing in-between nearly flat laminar regions. Once again, the quasiperiodic oscillations that comprised the laminar regions during intermittency in the 2 mm gap Couette are absent [12]. Instead we see small-amplitude oscillations with $a_0 \approx 0.8\%$ (indicated by arrows). This shear rate corresponds to point marked 5 on the flow curve and the vorticity structure is shown in Fig. 1 (a5). The experiment was done for two incident laser polarizations at +45° and −45° to the flow and the dashed line in Fig. 2(b) indicates the time at which the incident polarization was changed. The corresponding vorticity structure is shown in Fig. 2 (b1 and b2, respectively) (see movie [17]). Figure 2 (b3) is the sum of Figs. 2 (b1) and 2 (b2) and is identical to the intensity profile seen for a incident laser polarization parallel to the flow. To capture the dynamics, we have shown the time evolution of the interface separating adjacent vorticity bands as a space-time plot (STP) in Fig. 2(c). For ease of viewing, we plot only one interface for the two incident polarizations which are denoted by the thick white lines in Figs. 2 (b1) and 2 (b2), respectively. During chaos, the wavelength of the vorticity structures along $\nabla \times \mathbf{v}$ is preserved. But temporally, the structures as a whole travel up and down along the vorticity, by almost one wavelength, in an aperiodic manner—*spatially periodic, temporally chaotic* [first chaotic region Fig. 2(c), polarization +45° to flow]. This implies the instantaneous local orientation oscillates between +45° and −45° to flow. After the chaotic-laminar transition, the temporally aperiodic motion stops and the interface slowly moves up the gap and settles down [first laminar region Fig. 2(c), polarization +45° to flow]. This corresponds to the slow increase in the stress following the chaotic burst [Fig. 2(b)]. For the rest of the laminar region, the interface position shows small-amplitude oscillations along the $\nabla \times \mathbf{v}$ [sawtooth structure in STP, second laminar region Fig. 2(c)] and there is a direct correspondence with the small-amplitude oscillations in the laminar region of the stress. We should keep in mind that stress variations are small ($a_0 \approx 0.8\%$) and the interface motion still correctly captures this. The spatiotemporal oscillations of the local orientational order thus completely determine the temporal behavior of the stress in line with theoretical predictions [8]. At higher shear rates, the spa-

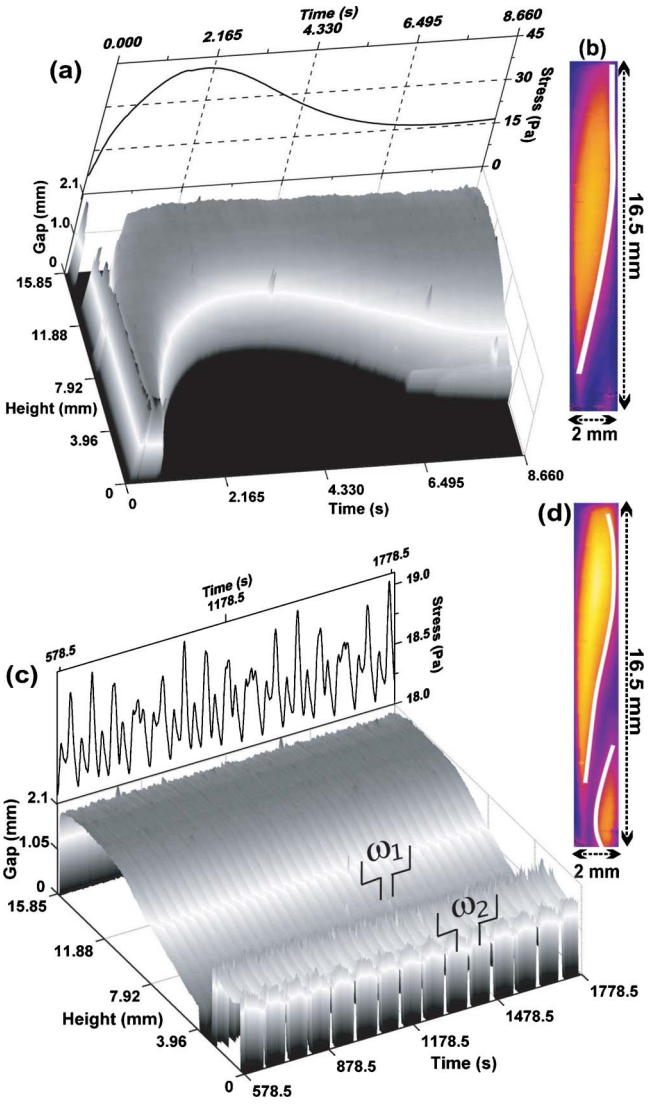

FIG. 3. (Color online) (a) Top panel: Transient response at $\dot{\gamma}=7$ s^{-1} in the 2 mm gap Couette cell. (b) Typical scattered intensity; the thick white line is the interface position represented as a STP in the bottom panel of (a). (c) Top panel: Long time dynamics at $\dot{\gamma}=7$ s^{-1}. (d) Typical scattered intensity; the thick white lines are the interface positions represented as a STP in the bottom panel of (c).

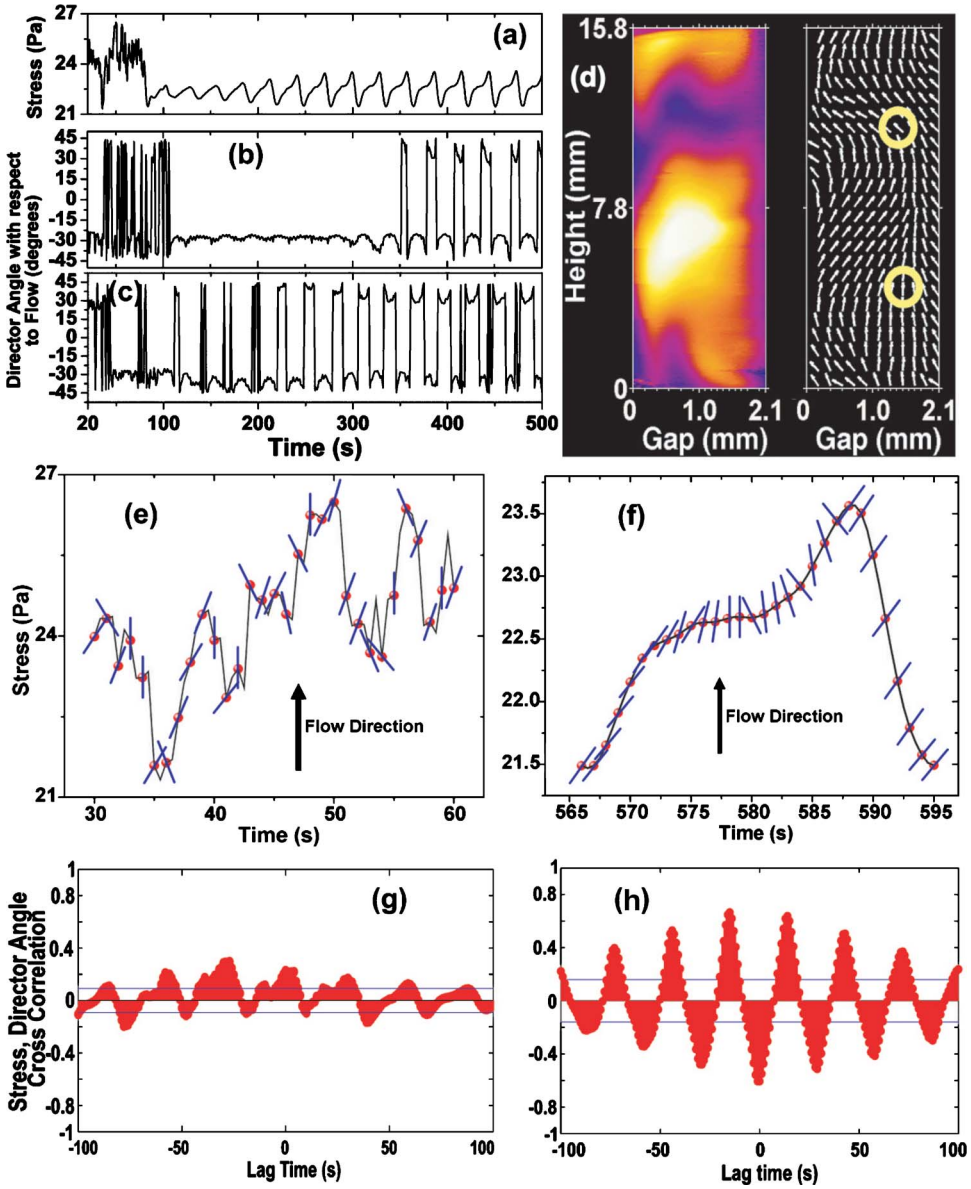

FIG. 4. (Color online) (a) Stress time series at $\dot{\gamma}=13.5\ s^{-1}$ in the 2 mm gap Couette cell. (b) Nematic director dynamics averaged over the position denoted by the top circle in (d) (ii). (c) Nematic director dynamics averaged over the position denoted by the bottom circle in (d) (ii). (d) (i) typical snapshot of the scattered intensity. (ii) shows the corresponding local nematic orientational order obtained from the scattered intensity. The director $\hat{\mathbf{n}}$ lies in the $(\mathbf{v},\nabla\mathbf{v})$ plane and points into the plane of the figure (shown along the $\nabla\times\mathbf{v}$ plane purely for representation). (e) and (f) show the nematic orientation (shown as rods), with respect to the flow, overlaid on the stress plot in the chaotic and laminar region, respectively. (g) and (h) show the cross correlations of (b) and (c) with (a), respectively.

tiotemporal dynamics and the stress are chaotic [12].

For the remainder of this paper, we will focus on the stress relaxation measurements in the 2 mm gap Couette cell. The flow curves in the 2 mm and 1 mm gap Couette are similar in shape but the absolute values are slightly different. The vorticity structures in this case are similar to that observed in the 1 mm gap shear cell, except that the wavelength of the vorticity bands in the 2 mm gap is approximately twice the 1 mm gap. Figure 3(a) shows the transient stress response on application of a step shear rate ($\dot{\gamma}=7\ s^{-1}$). The stress shows an overshoot followed by a weak undershoot [18]. The vorticity structures (captured at 30 Hz) appear from the bottom of the Couette cell and grow in intensity. The thick white line in Fig. 3(b) shows the interface profile whose evolution is shown as a STP in the bottom panel of Fig. 3(a) (incident laser polarization +45° to flow). For the first 2 s, the interface grows from the bottom of the shear cell and rapidly travels up along the $\nabla\times\mathbf{v}$ and this corresponds to the initial rapid increase in stress. From $\approx$2–6.5 s, the interface travels down along $\nabla\times\mathbf{v}$ followed by a short travel up and this corresponds to the undershoot seen in the stress. Throughout the transient, the shape of the interface across the gap remains unchanged (see Ref. [17]). Figure 3(c) (top panel) shows the stress dynamics at the same shear rate for long times. The signal resembles a beat pattern and a Fourier decomposition reveals that the signal is quasiperiodic with primary frequencies centered around ($\omega_1=0.012$ Hz and $\omega_2=0.027$ Hz) [12]. The bottom panel of Fig. 3(c) shows the STP of the two interfaces [denoted by the thick white lines in Fig. 3(d)] (see Ref. [17]). Although a single interface captures the essentials, we have plotted two for the sake of clarity. The STP of the interface clearly shows a corrugated surface and the periodicity corresponds to frequency ω_1 in the stress. This frequency component arises from the periodic motion of the interface along the $\nabla\mathbf{v}$ direction. The second interface captures ω_1 but one can also see the presence of a second frequency component which appears as periodic vertical slits in the STP. This frequency corresponding to ω_2 in the stress time series arises from the periodic motion of the interface along the $\nabla\times\mathbf{v}$ direction.

The dynamics we thus observe is far richer than the 1 mm gap Couette cell, where interface motion was restricted to the $\nabla \times \mathbf{v}$ direction. Also the quasiperiodic oscillations have an amplitude of about $a_0 \approx 5\%$. This clearly points out the crucial role played by the gap, a parameter hitherto glossed over, in determining the spatiotemporal dynamics of the nematic order and hence the stress [8].

Figure 4(a) shows a small section of the stress relaxation time series at a $\dot{\gamma}=13\ s^{-1}$. The time series captures the chaos-to-laminar transition and is characteristic of the type-II intermittency route to rheochaos [12]. Figure 4(d) (i) shows the scattered intensity profile (incident laser polarization +45° to flow) in the chaotic regime. The interface profile between adjacent vorticity bands is more complex than those seen at lower shear rates [Fig. 3(b)] and we are unable to clearly represent the dynamics of the interface as a STP. To determine the local nematic orientation across the gap of the Couette cell, we do the following: the images acquired are from a polarized scattering experiment. Thus the totally bright regions in the image for a given incident laser polarization with respect to the flow arises from nematics that are locally oriented parallel to the incident laser polarization and totally dark regions correspond to local nematic orientation that is perpendicular to the incident laser polarization. From the scattered intensity images, we know that the nematics in adjacent vorticity structures are oriented either at +45° or −45° to the flow. Thus, any intensity value in our grayscale images that lie in between those values can be mapped to an orientation $-45° < \theta < +45°$, where θ is the angle made by the nematic director $\hat{\mathbf{n}}$ to the flow $\mathbf{v}$. The nematic orientation, averaged over a small local region, over the gap corresponding to Fig. 4(d) (i) is shown in Fig. 4(d) (ii). The director $\hat{\mathbf{n}}$ lies in the $(\mathbf{v},\nabla\mathbf{v})$ plane and points into the plane of the figure (it is shown to point in the $\nabla \times \mathbf{v}$ plane purely for representation [Fig. 4(d) (ii)] (see Ref. [17]). We now track the dynamics of the director in a local region [indicated by the top circle in Fig. 4(d) (ii)] for a 30 s time interval during chaos and for a single laminar oscillation. Figures 4(e) and 4(f) show the director orientation (shown as rods) with respect to the flow overlaid on the stress plot in the chaotic and laminar regions, respectively. Figures 4(b) and 4(c) show the dynamics of the nematic orientation angle with respect to the flow for two regions denoted by the circles in Fig. 4(d) (ii). Although there exists strong correlations between Figs. 4(b) and 4(c) and the corresponding stress time series shown in Fig. 4(a), the magnitude of the nematic orientation dynamics is different in these two regions and captures the spatiotemporal essence of the problem. Since linear cross correlations procedures are in principle not applicable to nonlinear problems, an issue we have addressed in an earlier work [13], we are unable to show good correlations between the stress and the nematic orientation dynamics in the chaotic region of the time series. Figures 4(g) and 4(h) show the cross correlation between the stress and the nematic orientation angle at various time lags. The correlations between the stress and the nematic order are evident.

IV. INTERPRETATION

Our experiments thus clearly show the presence of vorticity structures in a shear-thinning wormlike micellar fluid. A possible explanation that might account for this finding is a recent mechanism proposed by Fielding [19]. Here, a secondary linear instability [20] arising from normal stress differences across the band interface leads to vorticity stress structuring superposed on gradient bands. This is accompanied by 2D Taylor-like velocity rolls with wavelength comparable to the gap width and these would show up as birefringent stripes stacked along the vorticity in a polarized light scattering experiment [21]. The flow velocity and the roll velocity are in mutually perpendicular directions and adjacent rolls have their velocities pointing in opposite directions along $\nabla\mathbf{v}$. Thus the local orientation in adjacent rolls will be along the resultant velocities that are symmetric with respect to the flow in the $(\mathbf{v},\nabla\mathbf{v})$ plane, respectively [Fig. 5(b)]. The birefringent stripes seen in our experiments [Fig. 5(a)] are in qualitative agreement with theory. A robust test to determine if the above model captures our observations on this specific micellar system would involve carrying out spatially resolved velocity measurements to relate the birefringence to the local velocity. An underlying assumption in the theoretical model that leads to 2D Taylor-like rolls is that the fluid is gradient-banding. We do not see clear evidence of gradient shear bands in our experiment before the onset of roll structures in the nonlinear region of the flow curve. This might be because the gradient band interface is close to the inner rotating wall and our polarized scattering experiment is unable to access this. In light of previous experiments by Fischer *et al.* [22], where it was shown that birefringence bands do not necessarily correspond to shear bands, velocity profile measurements are once again necessary to show that the fluid is gradient banding and to access the velocity profile within the rolls. This is beyond the scope of the present work and is an issue we intend to address in a future work. In contradiction to the theoretical model [19] are our findings that show a decrease in the wavelength of the rolls with

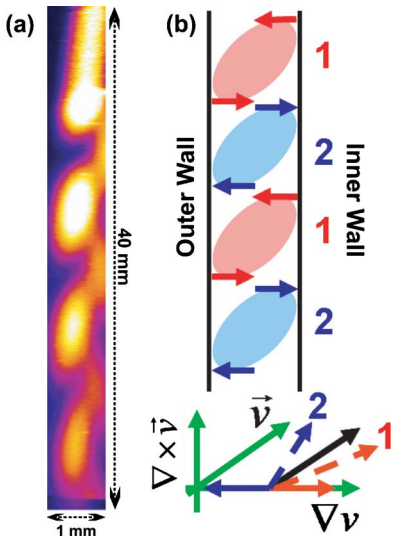

FIG. 5. (Color online) (a) Typical roll structure seen in the experiment for a 1 mm gap Couette cell. (b) Taylor-like velocity rolls. The flow velocity is shown by a black arrow and the resultant velocity for adjacent rolls denoted 1 and 2 is shown by dashed arrows.

increasing shear rates [Fig. 1 (a3–a5)] and the appearance of vorticity structures before the onset of the stress undershoot in the transient response [Fig. 3(a)]. Most importantly, the theoretical model also does not predict the observed spatial dynamics of the rolls. This may not be surprising since the model does not take into account flow-concentration coupling.

V. CONCLUSIONS

In conclusion, we have quantified the complete spatiotemporal dynamics of the local orientation, over the entire gap of the Couette cell, en route to rheochaos. A surprising finding is that the orientational order shows vorticity structuring in a gradient banding shear-thinning wormlike micellar gel and is quite contrary to the orientational ordering expected in conventional gradient banding [2,3]. This vorticity structuring is seen as birefringent stripes corresponding to local orientational order at +45° and −45° to the flow, and this is qualitatively similar to the recent prediction of 2D Taylor-like rolls in a shear-thinning fluid [19]. Most importantly, the complexity of the temporal stress dynamics that is a manifestation of the spatial dynamics of the vorticity structures along the vorticity and/or the shear gradient direction depends crucially on the system size [8]. Although the theoretical model [19] in its present form does not predict the transient response and the observed spatial roll dynamics, it does suggest a novel mechanism for triggering flow instabilities in complex fluids, and this is borne out by our experiments. The possible link between our findings and elastic Taylor-Couette instabilities [21] in polymeric fluids remains to be explored.

ACKNOWLEDGMENTS

We would like to thank Professor Sriram Ramaswamy for fruitful discussions. A.K.S. thanks the Council of Scientific and Industrial Research (CSIR), Government of India for support.

[1] R. Bandyopadhyay, G. Basappa, and A. K. Sood, Phys. Rev. Lett. **84**, 2022 (2000); R. Bandyopadhyay and A. K. Sood, Europhys. Lett. **56**, 447 (2001); P. Fisher, Rheol. Acta **39**, 234 (2000); A. S. Wunenburger, A. Colin, J. Leng, A. Arneodo, and D. Roux, Phys. Rev. Lett. **86**, 1374 (2001); J.-B. Salmon, A. Colin, and D. Roux, Phys. Rev. E **66**, 031505 (2002); L. Courbin, P. Panizza, and J.-B. Salmon, Phys. Rev. Lett. **92**, 018305 (2004); L. Bécu, S. Manneville, and A. Colin, *ibid.* **93**, 018301 (2004); D. Lootens, H. Van Damme, and P. Hébraud, *ibid.* **90**, 178301 (2003).

[2] N. A. Spenley, M. E. Cates, and T. C. B. McLeish, Phys. Rev. Lett. **71**, 939 (1993).

[3] R. Makhloufi, J. P. Decruppe, A. Ait-Ali, and R. Cressly, Europhys. Lett. **32**, 253 (1995); R. W. Mair and P. T. Callaghan, *ibid.* **36**, 719 (1996).

[4] M. R. López-Gonzaleź, W. M. Holmes, P. T. Callaghan, and P. J. Photinos, Phys. Rev. Lett. **93**, 268302 (2004); W. M. Holmes, M. R. López-Gonzaleź, and P. T. Callaghan, Europhys. Lett. **64**, 274 (2003); J.-B. Salmon, S. Manneville, and A. Colin, Phys. Rev. E **68**, 051504 (2003).

[5] P. Fischer, Rheol. Acta **41**, 35 (2002).

[6] A. Aradian and M. E. Cates, Europhys. Lett. **70**, 397 (2005).

[7] S. M. Fielding and P. D. Olmsted, Phys. Rev. Lett. **92**, 084502 (2004).

[8] B. Chakrabarti, M. Das, C. Dasgupta, S. Ramaswamy, and A. K. Sood, Phys. Rev. Lett. **92**, 055501 (2004).

[9] S. M. Fielding and P. D. Olmsted, Phys. Rev. Lett. **96**, 104502 (2006).

[10] S. Lerouge, M. Argentina, and J. P. Decruppe, Phys. Rev. Lett. **96**, 088301 (2006).

[11] K. Kang, M. P. Lettinga, Z. Dogic, and Jan K. G. Dhont, Phys. Rev. E **74**, 026307 (2006).

[12] R. Ganapathy and A. K. Sood, Phys. Rev. Lett. **96**, 108301 (2006).

[13] R. Ganapathy, G. Rangarajan, and A. K. Sood, Phys. Rev. E **75**, 016211 (2007).

[14] R. Ganapathy and A. K. Sood, Langmuir **22**, 11016 (2006).

[15] S. M. Fielding and P. D. Olmsted, Eur. Phys. J. E **11**, 65 (2003); E. Helfand and G. H. Fredrickson, Phys. Rev. Lett. **62**, 2468 (1989).

[16] The polarization-dependent scattering due to the spatial ordering of oriented structures is termed "form conservative dichroism" [G. G. Fuller, Annu. Rev. Fluid Mech. **22**, 387 (1990)].

[17] See EPAPS Document No. E-PLEEE8-78-162808 for movies of spatiotemporal dynamics during flow and stress relaxation measurements. For more information on EPAPS, see http://www.aip.org/pubservs/epaps.html.

[18] R. Ganapathy and A. K. Sood, J. Non-Newtonian Fluid Mech. **149**, 78 (2008).

[19] S. M. Fielding, Phys. Rev. E **76**, 016311 (2007).

[20] S. M. Fielding, Phys. Rev. Lett. **95**, 134501 (2005).

[21] R. G. Larson, Rheol. Acta **31**, 213 (1992).

[22] E. Fischer and P. T. Callaghan, Europhys. Lett. **50**, 803 (2000).